The Secondary Emission Model: An Influence of the Dust Grain Shape

I. Richterová, M. Beránek, Z. Němeček, J. Pavlů, J. Šafránková

Charles University, Faculty of Mathematics and Physics, Prague, Czech Republic

Abstract. Dust grains are bombarded by hot electrons in various space and terrestrial plasmas. Primary electrons can release low-energy secondary electrons and/or they can be scattered prior being completely slowed-down inside a grain. For convex grains, the secondary and scattered yields of omnidirectional primary electrons do not depend on a grain shape unless the primary electron penetration depth is comparable with the grain size. For glassy grains, the shape effect becomes negligible for grains larger than 1 μm and 30 μm when irradiated by 1 keV and 10 keV primary electrons, respectively. In this paper, we utilize our numerical model of secondary electron emission from small dust grains to study local yield variations across grain surfaces.

Introduction. Dust grains are an integral part of both laboratory and space plasmas and serve as a sink for recombining charged particles. Beside the particle attachment, dust grains are (dis)charged by several kinds of particle- and field-induced emissions [1, 2, e.g.]. Among them, secondary electron emission is always present since secondary and/or scattered primary electrons are released from the grain surface at any primary electron energy [3]. Fluxes of the lower-energy electrons continue even if grains are charged to equilibrium potentials. These electrons can affect the surrounding plasma parameters and imping other dust grains. The value of the total secondary electron yield crosses unity (and the sign of resulting current becomes positive) at about 30 eV and 90 eV for insulating and conducting grains, respectively [4]. For higher electron energies, it can or cannot cross unity again depending on a grain material, size, and shape [5]. Such hot electrons are present in tokamaks or electron beam experiments as well as in planetary magnetospheres or even within the solar wind.

In our dust group, we have performed both laboratory and numerical studies of charging of dust grains irradiated by a monoenergetic hot electron beams [5]. The secondary electron model [6, 7] based on approaches designed for the scanning electron microscopy [8, 9, e.g.] describes the electron–solid interaction. Primary electron paths inside the grain are traced and excited material electrons propagate to the surface according to exponential decay. The model fits our experimental data from spherical samples of different materials well. Although it is hard to prepare well defined samples of nonspherical dust grains, our simulation model deals, in principle, with grains of arbitrary shapes. Here, we compare local secondary and scattered yields of submicron glassy grains shaped to spheres, cubes and tetrahedra.

Results. As a sample material, we have chosen a glass based mineral which can be found in

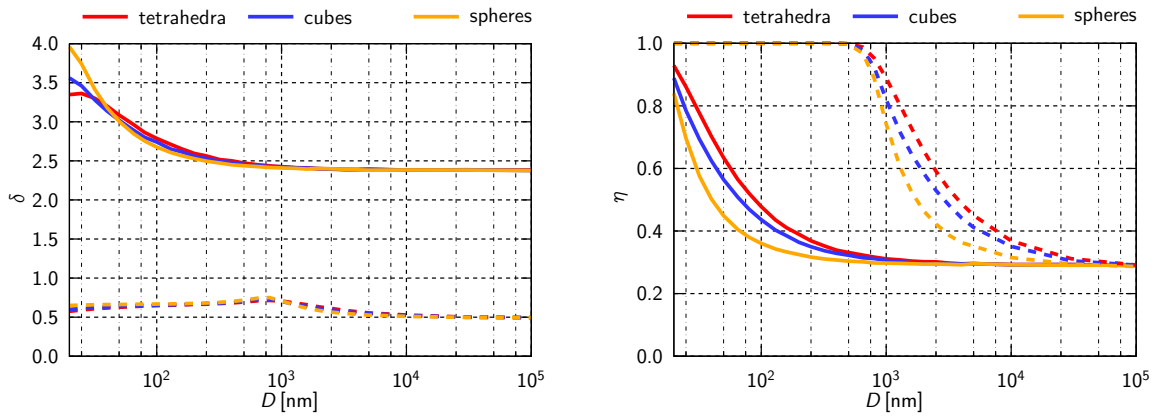

Figure 1: Modeled mean secondary (left) and scattered (right) electron yields as a function of a grain effective size for various grain shapes. Full and dashed line correspond to the 1 keV and 10 keV primary electrons, respectively.

both crystalline and amorphous forms. The composition of simulated grains corresponds to an average composition of lunar highlands type (LHT) simulant grains [10]. The secondary electron yield induced by omnidirectional electrons reaches the maximum value 3.1 at 390 eV for large convex LHT grains [11]. The scattered yield increases to 0.3 at 300 eV and then remains rather constant. For smaller grains, a penetration depth of primary electrons becomes comparable to the grain size and the scattered yield increases with energy again until it reaches unity. The smaller vertex angle a grain has the earlier the second increase occurs. When the scattered yield approaches unity, there is a corresponding subsidiary maximum of a secondary yield. The subsidiary maximum is more pronounced as it gets closer to the first maximum [11]. As an example, the size-dependencies of secondary and scattered electron yields for grains irradiated by 1 keV and 10 keV are shown in a Fig 1.

While values of a secondary yield and a scattered yield remain constant across the surface of spherical grains, they change close to edges. The probability that primary electron leave a grain rises towards edges. The secondary yield is proportional to the number of scattered electrons and depends on their energy. If the distance to the closest edge is a fraction of the attenuation length of secondaries (2 nm for LHT), the volume with excited electrons becomes smaller than the volume with a high escape probability and the secondary yield descends.

Local variabilities of the secondary yield and the scattered yield are plotted for cube-shaped grains in Fig 2. Grain masses corresponding to spherical grains of 20, 50, 130, and 2000 nm were chosen. A particular contour corresponding to a spherical grain value is drawn in each figure if possible.

As expected, the scattered yield reaches highest values at vertexes. It never cross unity since

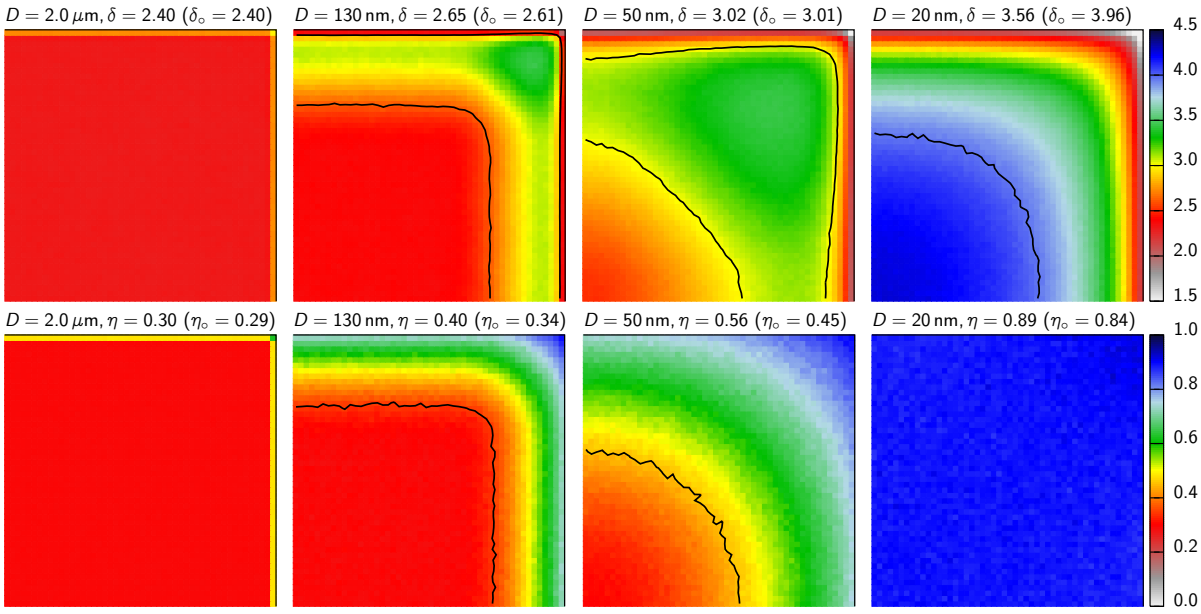

Figure 2: Trends of local secondary (top row) and scattered (bottom row) electron yields of 1 keV electrons for three different submicron cubes ($a = 0.805D$). The bottom left and the top right corner of each sketch represents the wall center and the cube vertex, respectively.

there is no directional fluxes to them. When the mean scattered yield approaches unity, the local density becomes more homogeneous. The local density of impinging electrons being later scattered exhibits a bit higher contrast (not plotted). Although the mean value of the scattered yields of cubes exceed that of spheres, its local value in the middle of the plain wall growths slower than that of curved surface.

Except the smallest grain, the secondary yield profiles have maxima close to (but not at) vertexes in accordance with the previous considerations. The scattered yield of the smallest grains peak at the wall center since the scattered electrons leaving here are most slowed. Since the spherical grain of the same mass brakes down primary electrons more effectively in this case, the mean value of the scattered yield reaches even lower value for the cube than for the sphere.

Fig 3 shows the secondary and scattered yield profiles for tetrahedral grains of the same mass as in Fig 2. Notice that the center-vertex contrast here is more pronounced comparing to cubes.

Summary. We have studied local distributions of secondary and scattered yields across surface of convex grains with etches. While the scattered yield peaks at the sharpest vertexes, the secondary yield is influenced by both, the number of scattered electrons and their actual energies. The obtained results are interesting, e.g., in the view of a particle induced desorption. Its yield depend on a particle species and its energy [12, and references therein]. Even in the case of a deeply frozen (upto 80 K) water ice, the yield reaches unity for 90 eV electrons. Thus, we

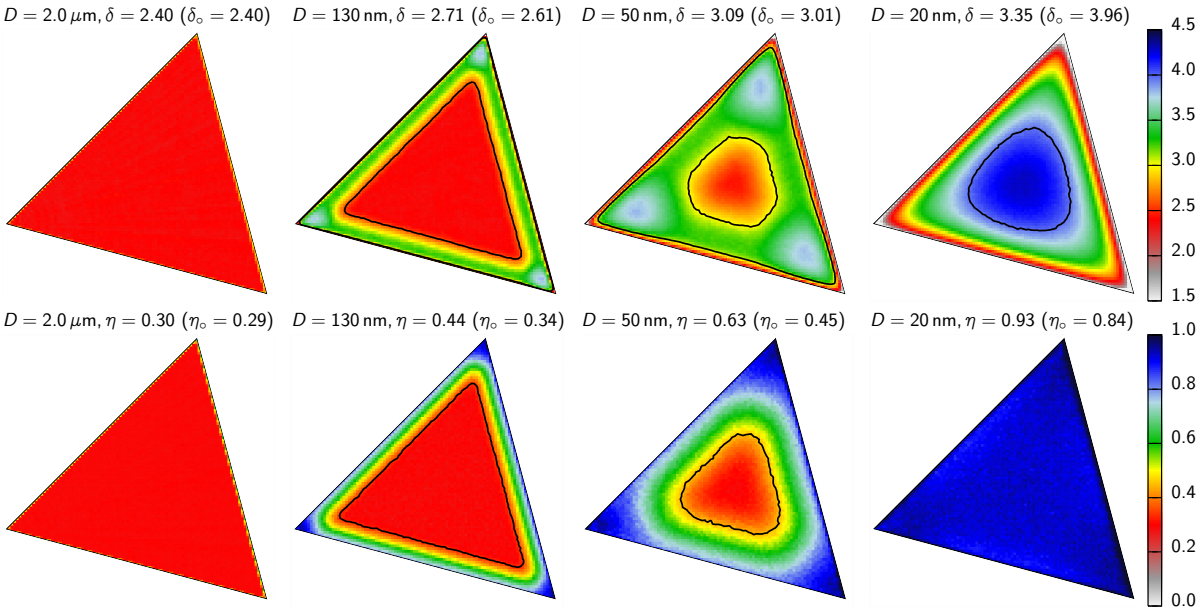

Figure 3: Trends of local secondary (top row) and scattered (bottom row) electron yields of 1 keV electrons for three different submicron tetrahedra ($a = 1.644D$).

plan to trace completely also tertiary electrons (i.e., Auger electrons, etc.) in the future work.

References

[1] Draine, B. and E. Salpeter, Astrophys. J., **231**(1), 77–94 (1979)

[2] Mann, I., A. Pellinen-Wannberg, E. Murad, O. Popova, N. Meyer-Vernet, M. Rosenberg, T. Mukai, A. Czechowski, S. Mukai, J. Šafránková, and Z. Němeček, Space Sci. Rev. **161**, 1–47 (2011)

[3] Bronstein, I. and B. Fraiman, Secondary Electron Emission (1969)

[4] Richterová, I., Thesis abstract, Charles University in Prague (2012)

[5] J. Pavlů, I. Richterová, Z. Němeček, J. Šafránková and I. Čermák, Faraday Discuss., **137**, 139–155 (2008)

[6] Richterová, I., J. Pavlů, Z. Němeček, and J. Šafránková, Phys. Rev. B, **74**(23) (2006)

[7] Richterová, I., M. Beránek, J. Pavlů, Z. Němeček, and J. Šafránková, Phys. Rev. B, **81**(7), 075406 (2010)

[8] P. Hovington, D. Drouin and R. Gauvin, Scanning, **19**(1), 1–14 (1997)

[9] Z. J. Ding and R. Shimizu, Scanning, **18**(2), 92–113 (1996)

[10] NU-LHT-2M material safety data sheet, USGS, Denver, CO, USA (2008)

[11] Richterová, I., M. Beránek, J. Pavlů, Z. Němeček, and J. Šafránková, Phys. Rev. B, submitted (2012)

[12] Johnson, R. E., Photolysis and radiolysis of water ice (2011)